Investigation of Free Singly and Doubly Charged Alkali Metal Sulfate Ion Pairs: $M^+(SO_4^{2-})$ and $[M^+(SO_4^{2-})]_2$ (M = Na, K)

Xue-Bin Wang,[†,‡] Chuan-Fan Ding,[†,‡] John B. Nicholas,*[,‡] David A. Dixon,[‡] and Lai-Sheng Wang*[,†,‡]

Department of Physics, Washington State University, Richland, Washington 99352, and W. R. Wiley Environmental Molecular Sciences Laboratory, Pacific Northwest National Laboratory, MS K8-88, P.O. Box 999, Richland, Washington 99352

Received: January 6, 1999; In Final Form: March 16, 1999

We present a combined experimental and theoretical investigation of alkali metal sulfate ion pairs and their doubly charged dimers in the gas phase: $Na^+SO_4^{2-}$, $K^+SO_4^{2-}$, $(NaSO_4)_2^{2-}$, $(KSO_4)_2^{2-}$, and $NaK(SO_4)_2^{2-}$. We produced these anions using an electrospray technique and measured their photoelectron spectra at three photon energies, 355, 266, and 193 nm. The photoelectron spectra of each anion exhibit two detachment features, which approximately correspond to detachment from the HOMO and HOMO-1 of the SO_4^{2-} group perturbed by the cations. The electron binding energies of the dimer dianions are lower than those of the monomers because of the strong electron−electron repulsion in the dianions. We also observed the repulsive Coulomb barriers in the dianions and their effects on the photodetachment spectra. We used density functional theory and ab initio molecular orbital theory to obtain the geometric and electronic structure of the ion pairs. The calculated electron binding energies and orbital energy separations are in reasonable agreement with the experimental values. We found that the MSO_4^- ion pairs have C_{3v} symmetry with a C_{2v} structure slightly higher in energy. In the dimer dianions the two alkali metal cations bridge the two SO_4^{2-} groups.

I. Introduction

Sulfate (SO_4^{2-}) is one of the most important inorganic anions in the liquid and solid phase. There have been extensive experimental studies of sulfate, mainly via photochemistry of sulfate solutions[1] and vibrational spectroscopy of molten sulfates.[2] The bond length,[3] vibrational frequencies,[2,4] effective ionic radii,[5] and electronic polarizabilities[5,6] of SO_4^{2-} in the condensed phase have been determined experimentally. The molecular orbitals of the tetrahedral SO_4^{2-} were also studied,[7,8] and isolated SO_4^{2-} was found to be unstable to autodetachment in the gas phase.[9] Rather, several water molecules are required to stabilize SO_4^{2-}.[10] Therefore, it appears that free SO_4^{2-} cannot be studied experimentally. The goal of this work is to investigate SO_4^{2-} stabilized by a countercation (Na^+ and K^+) instead of water or other solvent molecules. Such ion-pair formation is present in the aqueous solutions and is important to environmental systems. We present the first experimental observation of such ion pairs and their dimers in the gas phase, combined with theoretical studies of these novel species.

Contact ion pairs, common in electrolyte solutions,[11] can be generally viewed as anions perturbed electrostatically by cations. Ion-pair interactions are important in electrolyte solutions and play significant roles in determining the stability, structure, and function of biomolecules,[12] as well as many other systems.[13,14] There have been extensive Raman spectroscopy studies on the formation and properties of contact ion pairs in dilute electrolyte solutions.[15,16] These studies found that the vibrational frequencies of the anionic part of an ion pair were shifted relative to those of the free anion. There are also significant experimental efforts directed toward the development of very weakly coordinating ions.[17] Despite the importance of ion pairs in solution, to our knowledge the only previous gas-phase work on the complexes studied here is a mass spectrometric study of KSO_4^-.[18]

In this paper, we report a photoelectron spectroscopy (PES) study of $M^+SO_4^{2-}$ (M = Na, K) using a newly developed apparatus with a magnetic-bottle time-of-flight (TOF) photoelectron analyzer and an electrospray ionization (ESI) source. We also observed doubly charged dimers of the ion pairs, $(NaSO_4)_2^{2-}$, $(KSO_4)_2^{2-}$, and $NaK(SO_4)_2^{2-}$. PES is an ideal technique to investigate the intrinsic properties of free anions. For singly charged anions, PES provides direct measurements of the electron affinities (EAs) of the corresponding neutral species, as well as information about their low-lying electronic states. PES is also well-suited for studying the gas-phase stability and intramolecular electrostatic interactions of multiply charged anions, as we have demonstrated recently.[19−22] We found that the PES features of the dimers of the ion pairs are nearly identical to those of the monomers, although shifted to lower binding energies because of the intramolecular Coulomb repulsion in the dianions. We carried out density functional theory (DFT) and ab initio molecular orbital calculations to elucidate the geometric and electronic structure of the alkali metal sulfate ion pairs and their dimers. The electron binding energies were computed and compared to the experimental measurements. We found that both $NaSO_4^-$ and KSO_4^- have a C_{3v} ground-state structure with a C_{2v} structure slightly higher in energy. The structure of the ion-pair dimers has the two alkali metal cations sandwiched by the two SO_4^{2-} ions.

The paper is organized as follows. In section II, the experimental aspects will be briefly described, whereas section III provides a brief description of the theoretical methods. The experimental and theoretical results are presented and discussed in section IV. A brief summary is given in section V.

[†] Washington State University.
[‡] Pacific Northwest National Laboratory.

10.1021/jp990071o CCC: $18.00
Published on Web 04/16/1999

II. Experimental Details

The experiments were carried out with an apparatus that includes a magnetic-bottle TOF photoelectron analyzer and an ESI source. Details of this apparatus have been reported recently,[23] and only a brief description of the experimental procedures is given here. To produce the desired anions, we used a 10^{-4} M solution of the corresponding salts (Na_2SO_4 and K_2SO_4) at pH ~7 in a water/methanol mixed solvent (2/98 ratio). The solution was sprayed through a 0.01 mm diameter syringe needle at ambient atmosphere and −2.2 kV high voltage. Negatively charged molecular ions emerging from a desolvation capillary were guided by a radiofrequency-only quadrupole ion guide into an ion trap, where the ions were accumulated for 0.1 s before being pushed into the extraction zone of a TOF mass spectrometer. The ion trap was maintained at room temperature, and the temperature of the stored ions was expected to be at or slightly above room temperature.

In each PES experiment, the anions of interest were mass-selected and decelerated before being intercepted by a laser beam in the detachment zone of the magnetic-bottle photoelectron analyzer. For the current study, the 355 (3.496 eV) and 266 nm (4.661 eV) photons from a Nd:YAG laser and the 193 nm (6.424 eV) photons from an ArF excimer laser were used for photodetachment. The photoelectrons were collected at nearly 100% efficiency by the magnetic-bottle and analyzed in a 4 m long TOF tube. The photoelectron TOF spectra were then converted to kinetic energy spectra, calibrated by the known spectra of I^- and O^-.[24] The binding energy spectra were obtained by subtracting the kinetic energy spectra from the corresponding photon energies. The energy resolution was about 11 meV (fwhm) at 0.4 eV kinetic energy, as measured from the spectrum of I^- at 355 nm.[23]

III. Theoretical Details

We used theoretical calculations to determine the geometry and electronic structure of the ion pairs and as verification of our interpretation of the PES spectra. All the ion pairs were optimized with DFT. The optimizations used the hybrid B3LYP exchange-correlation functional.[25] For H, O, and S we used the tzvp+ basis set, which is derived from the DFT-optimized tzvp basis set of Godbout and co-workers[26] with the addition of a diffuse s (H, O, and S) and p (O and S only) function. The exponents of the diffuse functions were derived from an even-tempered expansion of the outermost functions in the original basis set. For Na we used the TZ94 basis set from the DGauss program library.[27] This basis set had the same size as tzvp and was also optimized for DFT calculations. A diffuse s and p were also added to the Na basis set. For K, we used the valence basis set and effective core potential (ECPs) of Hay and Wadt.[28] The Hay−Wadt valence basis set is a (5s5p)/[3s3p] contraction to which we added the energy-optimized polarization function (exponent of d function = 0.19) suggested by Glendening and co-workers.[29] Relativistic (mass-velocity and Darwin) corrections are included in the K ECP. The Hay−Wadt formalism treats the (n − 1) shell of core electrons explicitly, while representing the rest of the core by the ECP. For simplicity we will refer to this collection of basis sets as tzvp+. Frequencies were calculated for all species to verify that the geometries were minima on the potential energy surface.

Following the DFT optimizations, single-point energies were obtained for the smaller systems ($NaSO_4$ and KSO_4) using coupled cluster theory with perturbative triples (CCSD(T)) and the 6-311+G* basis set. Energies from the other correlation treatments obtained from the CCSD(T) calculations (MP2, MP4-(sdq), and CCSD) are also reported. The core electrons were frozen in the CCSD(T) calculations. The vertical detachment energy (VDE) was taken as the difference in total energy between the anion and the corresponding neutral molecule at the anion geometry. The reported adiabatic detachment energy (ADE) is the difference in total energy between the optimized geometries of the anion and neutral. Partial atomic charges obtained from a Mulliken population analysis[30] are presented. We used Gaussian94 for all the calculations reported here.[31]

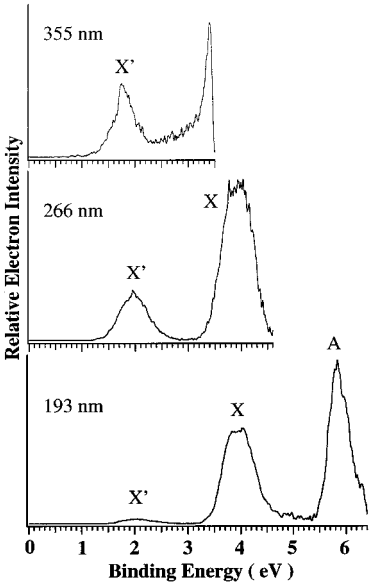

Figure 1. Photoelectron spectra of $NaSO_4^-$ at 193, 266, and 355 nm. Note the X′ peak at 355 nm is shifted to lower binding energy by 0.2 eV compared to that of the 266 and 193 nm spectra. The X′ peak is due to $[NaSO_4]_2^{2-}$.

IV. Results and Discussion

1. $Na^+SO_4^{2-}$ and $K^+SO_4^{2-}$. Figure 1 presents the photoelectron spectra of $NaSO_4^-$ measured at 355, 266, and 193 nm. The 193 nm spectrum shows three well-separated and rather broad features, labeled X′, X, and A. The intensity of the X′ feature is unusually low. The 266 and 355 nm spectra were measured to improve the resolution of the X′ and X features, although no fine features were resolved. Surprisingly, the PES signals corresponding to the X′ peak taken at 355 nm are much weaker than the signals obtained at 266 and 193 nm under similar experimental conditions (detachment laser fluxes and mass signals). We had to accumulate 4 times more total laser shots at 355 nm in order to obtain count rates comparable to the 266 and 193 nm measurements. Moreover, the position of the X′ peak at 355 nm was shifted to lower binding energy by about 0.2 eV. Similar observations were previously attributed to the repulsive Coulomb barrier in doubly charged anions.[22,32] In the current case, the X′ feature had to be from either a doubly or multiply charged anion that has the same mass-to-charge ratio (m/z) as $NaSO_4^-$, most likely $[NaSO_4]_2^{2-}$, as will be shown below.

Figure 2 shows the photoelectron spectra of KSO_4^- measured at 355, 266, and 193 nm. Not surprisingly, very similar spectral features were observed for KSO_4^- as for $NaSO_4^-$, except that the binding energies of KSO_4^- are slightly lower. The intensity of the X′ feature is also slightly higher in the KSO_4^- spectra. The X′ feature in KSO_4^- showed the same characteristics at 355 nm as that of $NaSO_4^-$ and is most likely due to $[KSO_4]_2^{2-}$. The measured ADE's and VDE's for the features observed in Figures 1 and 2 are given in Table 1.

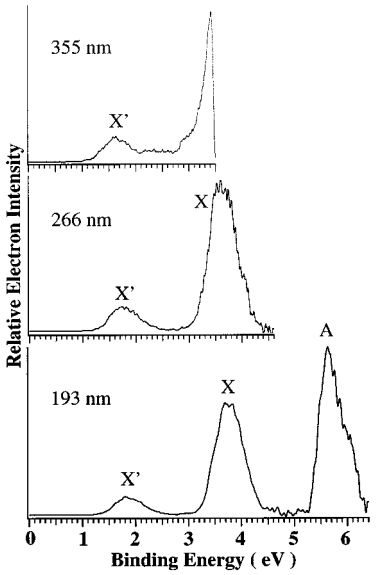

Figure 2. Photoelectron spectra of KSO_4^- at 193, 266, and 355 nm. Note the X′ peak at 355 nm is shifted to lower binding energy by 0.2 eV compared to that of the 266 and 193 nm spectra. The X′ peak is due to $[KSO_4]_2^{2-}$.

TABLE 1: Measured Adiabatic (ADE) and Vertical (VDE) Detachment Energies (eV) for $NaSO_4^-$, KSO_4^-, $(NaSO_4)_2^{2-}$, $(KSO_4)_2^{2-}$, and $NaK(SO_4)_2^{2-}$

		ADE	VDE
$NaSO_4^-$	X	3.5(0.1)	~3.9
	A	5.6(0.1)	5.84(0.05)
KSO_4^-	X	3.3(0.1)	~3.7
	A	5.4(0.1)	5.63(0.05)
$(NaSO_4)_2^{2-}$	X′	1.6(0.1)	1.96(0.08)
$(KSO_4)_2^{2-}$	X′	1.4(0.1)	1.75(0.08)
$NaK(SO_4)_2^{2-}$	X′	1.5(0.1)	1.9(0.1)
	A′	3.6(0.1)	~3.9

2. Doubly Charged Dimer Dianions: $[NaSO_4]_2^{2-}$, $[KSO_4]_2^{2-}$, and $NaK(SO_4)_2^{2-}$. Repulsive Coulomb Barriers and Electron Tunneling. To confirm the existence of doubly charged dimer anions, we sprayed a mixed solution of Na_2SO_4 and K_2SO_4, intending to produce $NaK(SO_4)_2^{2-}$, which has a *m*/*z* (127) different from both $NaSO_4^-$ (119) and KSO_4^- (135). The mixed dianion was indeed observed, though at much lower abundance than that of the monoanion. The PES spectra of $NaK(SO_4)_2^{2-}$ are shown in Figure 3 at 193, 266, and 355 nm. The sharp peaks in Figure 3 are due to I^-, which has an *m*/*z* ratio identical to that of $NaK(SO_4)_2^{2-}$. I^- was present as an impurity because we used it daily to calibrate our spectrometer and could not completely eliminate it from our system. Nevertheless, two other features were clearly observed in the 193 nm spectrum of $NaK(SO_4)_2^{2-}$, one starting at 1.5 eV (X′) and one starting at 3.6 eV (A). The latter is overlapped with one of the transitions from I^-. As expected, the X′ feature from the spectra of $NaK(SO_4)_2^{2-}$ is almost identical to that observed in the spectra of $NaSO_4^-$ and KSO_4^- and showed a similar spectral shift at 355 nm. Furthermore, the A′ feature of $NaK(SO_4)_2^{2-}$ was absent in the 266 nm spectrum. This absence, due to the repulsive Coulomb barrier which we will discuss below, further confirmed the dianionic nature of the species being photodetached.

As we reported recently in studies of multiply charged anions,[19−22,32] there is an essential difference between photodetachment from multiply and singly charged anions. In multiply charged anions, there exists a repulsive Coulomb barrier (RCB) against detachment of an electron because of the long-range

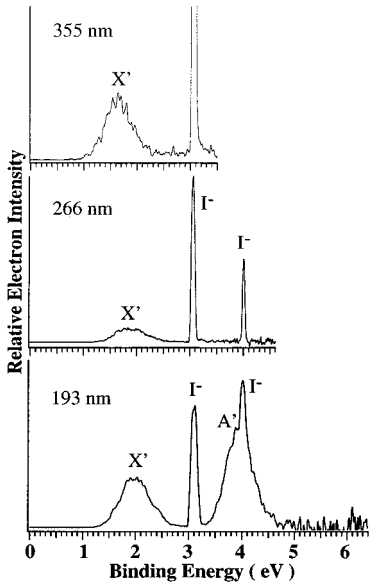

Figure 3. Photoelectron spectra of $[O_4S{\cdot}Na{\cdot}K{\cdot}SO_4]^{2-}$ (*m*/*z* = 127) at 193, 266, and 355 nm. The two sharp peaks are from I^- (*m*/*z* = 127) contamination. Note that the doubly charged anions have two detachment bands (X′ and A′) at 193 nm.

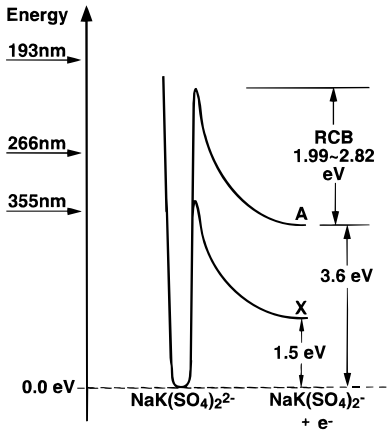

Figure 4. Schematic potential curves showing the repulsive Coulomb barriers (RCB) for electron detachment from $NaK(SO_4)_2^{2-}$. The barrier heights (1.99−2.82 eV) are assumed to be the same for the X and A channels, whose measured adiabatic detachment energies are given. The relative positions of the three detachment photon energies are indicated.

Coulomb repulsion between the outgoing electron and the remaining anion. When detachment photon energies are lower than the barrier height (but higher than the binding energy of the anions), PES signals can only be observed through electron tunneling. In the tunneling regime, we found that PES signals are usually considerably reduced and tend to shift to lower binding energies because of a strong dependence of tunneling probabilities on electron kinetic energies.[22,32] This appeared to be the case for the X′ feature in the 355 nm spectra for all three dimer dianions (Figures 1−3). When the photon energy is much lower than the barrier top for a given detachment channel, the tunneling probability becomes so small such that no photoelectron signals can be observed, even if the photon energy is higher than the electron binding energy. Such was the case for the A′ state of the mixed dimer dianion at 266 nm (Figure 3).

The RCB can be estimated from the photon energy dependence of the PES spectra, as shown schematically in Figure 4 for $NaK(SO_4)_2^{2-}$. Since the 355 nm (3.49 eV) photon energy was lower than the RCB to reach the ground state of the singly

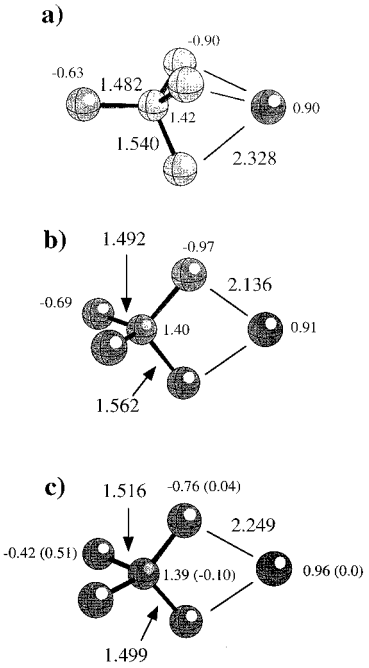

Figure 5. Geometries of $NaSO_4^-$ and $NaSO_4$ optimized at B3LYP.tzvp+: (a) C_{3v} $NaSO_4^-$; (b) C_{2v} $NaSO_4^-$; (c) C_{2v} $NaSO_4$. Selected bond lengths (in Å), Mulliken partial charges (|*e*|), and spin populations (in parentheses) are indicated.

charged dimer anions, the RCB can be estimated to be >1.89 eV in $[NaSO_4]_2^{2-}$, >2.09 eV in $[KSO_4]_2^{2-}$, and >1.99 eV in $NaK(SO_4)_2^{2-}$ (3.49 eV − ADE). Since the A feature was observed at 193 nm for $NaK(SO_4)_2^{2-}$, the RCB in $NaK(SO_4)_2^{2-}$ must be less than 2.82 eV, the photon energy (6.42 eV) minus the binding energy of the A state (3.6 eV). Thus, we can deduce that the RCB in $NaK(SO_4)_2^{2-}$ is 1.99 eV < RCB < 2.82 eV (Figure 4). As we reported recently,[20] the RCB is equivalent to the Coulomb repulsion of the excess charge in the dianion at its equilibrium configuration and is a fundamental property of a multiply charged anion. There should also be a second feature in the 193 nm spectra of $(NaSO_4)_2^{2-}$ (Figure 1) and $(KSO_4)_2^{2-}$ (Figure 2), analogous to the A′ feature in the 193 nm spectrum of $NaK(SO_4)_2^{2-}$ (Figure 3). However, these were probably overlapped with the X feature in each case and could not be identified. It should be noted that the expected second feature should not exist in the 266 nm spectra in Figures 1 and 2, owing to the RCB. We expected the RCB in $(NaSO_4)_2^{2-}$ and $(KSO_4)_2^{2-}$ to be similar to that in $NaK(SO_4)_2^{2-}$ (Figure 4).

3. Theoretical Results for $NaSO_4^-$ and KSO_4^-. We found two stable energy minima for $NaSO_4^-$. The lowest energy geometry at the B3LYP/tzvp+ level of theory has C_{3v} symmetry, with sodium coordinated to three oxygens (Figure 5a). In this geometry the three S−O bonds to the three oxygens coordinated to sodium are 0.06 Å longer than the other S−O bond. The three oxygens coordinated to sodium also have the most negative charge. A C_{2v} geometry, in which sodium is in close contact with two oxygens, is only 0.48 kcal/mol higher in energy at B3LYP/tzvp+ (Figure 5b). In this structure the two S−O bonds to the oxygens coordinated to sodium are 0.02 Å longer than the corresponding bonds in the C_{3v} complex, and the oxygens have a more negative charge. The distances between sodium and the oxygens are almost 0.2 Å shorter in the C_{2v} complex than they are in the C_{3v} complex, consistent with the change in coordination.

Considering this small difference in energy between the two conformers, we calculated the single-point energies for both symmetries at the CCSD(T)/6-311+G* level of theory. The other treatments of the correlation energy also indicated that the C_{3v} geometry of the anion is lower in energy, by 0.86 kcal/mol (MP2), 0.75 kcal/mol (MP4(sdq) and CCSD), and 0.82 kcal/mol (CCSD(T)). We expect that both species might be present in the experiments, partially accounting for the broadness of the peak at 4.0 eV (X, Figure 1).

TABLE 2: Comparison of the Calculated Adiabatic and Vertical Detachment Energies (eV) for $NaSO_4^-$ to That of the Experimental Results

	C_{3v}		C_{2v}	
	ADE	VDE	ADE	VDE
B3LYP/tzvp+	3.49	3.73	3. 47	3.62
MP2/6-311+G*[a]	3.34	3.59	3.30	4.43
MP4(sdq)/6-311+G*[a]	3.33	4.00	3.30	4.43
CCSD/6-311+G*[a]	3.25	3.99	3.22	4.25
CCSD(T)/6-311+G*[a]	3.22	3.81	3.18	4.10
exptl	3.5(0.1)	3.9	3.5(0.1)	∼3.9

[a] Calculated at the B3LYP/tzvp+ optimized geometry.

Neutral $NaSO_4$ has C_{2v} symmetry; a frequency calculation of the C_{3v} isomer gives two large imaginary eigenvalues. The C_{3v} geometry of the neutral is also higher in energy than the C_{2v} isomer at most levels of theory; 5.20 kcal/mol (B3LYP), 7.59 kcal/mol (MP4(sdq)), 8.92 kcal/mol (CCSD), and 6.44 kcal/mol (CCSD(T)). Only the MP2/6-311+G* single-point energy predicts that the C_{3v} isomer of the neutral is lower in energy, in this case by 1.12 kcal/mol. This anomalous result suggests that the MP2 level of theory is inadequate for the determination of the relative energies of the two isomers. We therefore calculated the ADE for both the C_{3v} and C_{2v} anions with regard to the energy of only the C_{2v} neutral. The B3LYP/tzvp+ optimized geometry of $NaSO_4$ is shown in Figure 5c. There are substantial changes in geometry between the C_{2v} anion and neutral. Most notably, the S−O bond distances of the oxygens coordinated to sodium are shorter (0.06 Å), whereas the other S−O bonds becomes longer. The Na−O distances also increase by ∼0.1 Å. The oxygens nearest the sodium have the largest negative charge; however, the unpaired electron is delocalized between the other two oxygens. The large geometry changes between the neutral and anions also contribute to the broadening of the 4.0 eV feature in the PES spectra (X, Figure 1).

The calculated ADEs are in reasonable agreement with experimental values (Table 2). The CCSD(T) values are somewhat lower than those obtained at B3LYP. As expected from the discussion above, the ADE for the C_{2v} isomer is only slightly lower than that of the C_{3v} isomer. In contrast, the predicted values of the VDE vary considerably, particularly for the C_{2v} anion. For the C_{3v} anion the lowest VDE is obtained with the MP2/6-311+G* single-point calculation, whereas the highest is predicted at the MP4 level. The MP2 VDE is the farthest away from the experimental value. The CCSD and CCSD(T) predictions bracket the experimental VDE. Even larger deviations are seen for the C_{2v} anion; in this case both the MP2 and MP4 VDEs appear to be too large by ∼0.5 eV. Only the B3LYP calculation predicts that the VDE is lower for the C_{2v} anion than it is for the C_{3v} anion.

Consistent with the similarities between the experimental spectra for $NaSO_4^-$ and KSO_4^-, we find that the complexes also have similar geometric and electronic structure. Thus, the KSO_4^- complex also has both a C_{3v} and C_{2v} isomer (parts a and b of Figure 6). In both cases the S−O bond lengths are within 0.007 Å of those of the corresponding Na complexes. As expected, the K−O distances are longer than the corresponding Na−O distances, consistent with the larger ionic radius

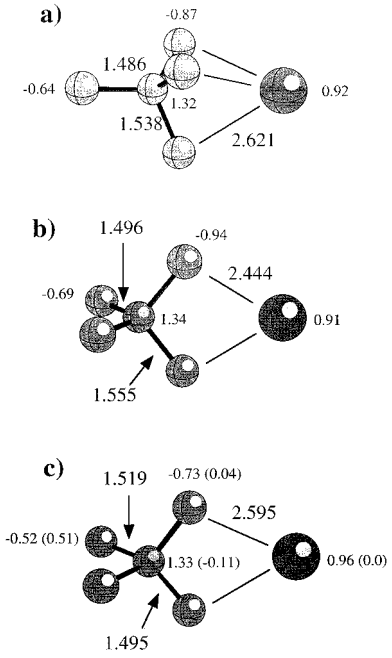

Figure 6. Geometries of KSO_4^- and KSO_4 optimized at B3LYP.tzvp+. (a) C_{3v} KSO_4^-, (b) C_{2v} KSO_4^-, (c) C_{2v} KSO_4. Selected bond lengths (in Å), Mulliken partial charges (|e|), and spin populations (in parentheses) are indicated.

TABLE 3: Comparison of the Calculated Adiabatic and Vertical Detachment Energies (eV) for KSO_4^- to That of the Experimental Results

	C_{3v}	
	ADE	VDE
B3LYP/tzvp+	3.01	3.40
MP2/6-311+G*[a]	3.00	3.71
MP4(sdq)/6-311+G*[a]	2.99	3.66
CCSD/6-311+G*[a]	2.91	3.57
CCSD(T)/6-311+G*[a]	2.87	3.36
exptl	3.3(0.1)	~3.7

[a] Calculated at the B3LYP/tzvp+ optimized geometry.

of potassium. The partial charges are also very similar to those calculated for the sodium complexes. Similar to $NaSO_4$ neutral, only a C_{2v} KSO_4 neutral was found (Figure 6c). The C_{2v} KSO_4 has bond lengths, partial charges, and spin populations that are also similar to $NaSO_4$.

For KSO_4^- the C_{2v} isomer is 3.30 kcal/mol higher in energy than the C_{3v} isomer. This energy difference is large enough that we choose to ignore the higher energy isomer in our calculation of the detachment energies. There is little difference in the values of the ADE calculated by the various methods (Table 3); the B3LYP/tzvp+ and CCSD(T)/6-311+G* values differ by ~0.1 eV. All of the calculated ADE's are ~0.3 eV lower than the experimental value. As was the case for $NaSO_4^-$, there is wider variation in the calculated values of the VDE. Again, the B3LYP and CCSD(T) values are very similar, whereas the other methods give VDEs that are greater by as much as 0.3 eV. The MP2, MP4, and CCSD predictions of the VDE are in good agreement with the experimental value. The B3LYP/tzvp+ and CCSD-(T)/6-311+G* predictions agree with each other but are ~0.3 eV lower than the experimental VDE. It appears likely that a better treatment of K, such as inclusion of core correlation, may be needed in order to obtain more accurate theoretical results.

4. Theoretical Results for $(NaSO_4)_2^{2-}$, $(KSO_4)_2^{2-}$, and $NaK(SO_4)_2^{2-}$. The B3LYP/TZVP+ optimized geometry of $(NaSO_4)_2^{2-}$ is shown in Figure 7a. The geometry of the C_{2h} dimer dianion resembles that of the C_{3v} monomer. Three of the oxygens of each SO_4^{2-} are coordinated to Na^+. The distances between oxygen and sodium are 0.02−0.04 Å longer than in the C_{3v} monomer. The S−O bond lengths differ by about 0.01 Å. Surprisingly, the two sodiums are only 2.953 Å apart. This distance is even shorter than the bond distance of 3.08 Å in Na_2,[33] suggesting that there is significant metal−metal bonding in this cluster. The partial charges are also similar to those of the C_{3v} monomer. The charge on sodium is essentially unchanged. The three oxygens coordinated with sodium have the greater negative charge. Apparently, the Coulomb repulsion between the sodiums is overcome by the Coulomb attraction between Na^+ and SO_4^{2-} in the dimer.

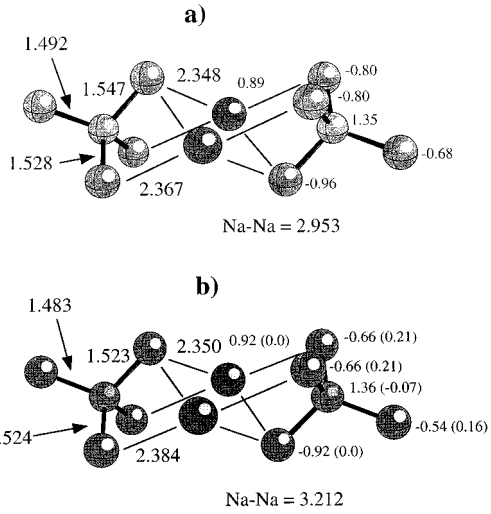

Figure 7. Geometries of $(NaSO_4)_2^{2-}$ (a) and $(NaSO_4)_2^-$ (b) optimized at B3LYP/tzvp+. Selected bond lengths (in Å), Mulliken partial charges (|e|), and spin populations (in parentheses) are indicated.

The geometry of $(NaSO_4)_2^-$ (Figure 7b) is qualitatively the same as that of the dianion. Loss of an electron results in increased distances between oxygen and sodium and an increased distance between the two sodiums. The bond distance of 3.21 Å is longer than that in Na_2, although the distance is not that much longer, suggesting the continuing presence of metal−metal interactions. The partial charges are also similar to those of the dianion. The most notable differences are the diminished charge on three of the oxygens of each SO_4 group. The unpaired electron is delocalized over these oxygens.

Figure 8a shows the B3LYP/tzvp+ optimized geometry of $(KSO_4)_2^{2-}$. The S−O bond lengths differ by less than 0.01 Å from those in $(NaSO_4)_2^{2-}$. As expected, the K−O and K−K distances are much longer than those in the Na−sulfate dimer, consistent with the larger size of the cation. The K−K distance in the dianion (3.52 Å) and the K−K distance in the monoanion (3.84 Å) are both shorter than the K−K distance in the bare K_2 dimer (3.90 Å),[33] again suggesting the presence of metal−metal interactions. Comparison with the geometry of the C_{3v} conformer of KSO_4^- indicates a greater lengthening of the K−O distances upon formation of the dimer than is predicted for $(NaSO_4)_2^{2-}$. The partial charges are also similar to those of $(NaSO_4)_2^{2-}$. There is a slightly greater positive charge on K, which is countered by a small increase in negative charge on the SO_4 groups. The optimized geometry of $(KSO_4)_2^-$ (Figure 8b) shows similar changes in geometry as predicted for $(NaSO_4)_2^-$, most notably the increased K−O and K−K distances. The partial charges and spin populations are also similar to those calculated for $(NaSO_4)_2^-$.

Parts a and b of Figure 9 show the B3LYP/tzvp+ optimized geometry of the mixed dimer. The results for the mixed dimer,

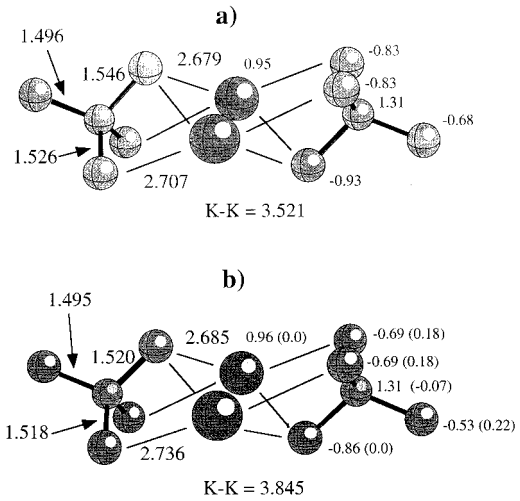

Figure 8. Geometries of $(KSO_4)_2^{2-}$ (a) and $(KSO_4)_2^-$ (b) optimized at B3LYP/tzvp+. Selected bond lengths (in Å), Mulliken partial charges (|*e*|), and spin populations (in parentheses) are indicated.

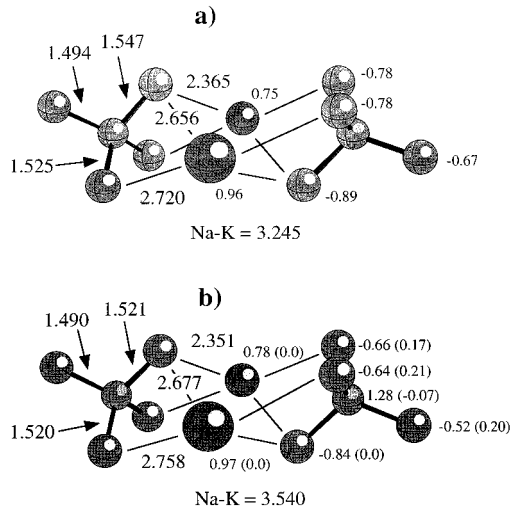

Figure 9. Geometries of $[(NaSO_4)(KSO_4)]^{2-}$ (a) and $[(NaSO_4)(KSO_4)]^-$ (b) optimized at B3LYP/tzvp+. Selected bond lengths (in Å), Mulliken partial charges (|e|), and spin populations (in parentheses) are indicated.

TABLE 4: Comparison of the Calculated Adiabatic and Vertical Detachment Energies (eV) for the Dimers Dianions to That of the Experimental Results

	$(NaSO_4)_2^{2-}$		$(KSO_4)_2^{2-}$		$(NaSO_4)(KSO_4)^{2-}$	
	ADE	VDE	ADE	VDE	ADE	VDE
B3LYP/tzvp+	1.13	1.27	0.86	1.13	0.99	1.10
exptl	1.6(0.1)	1.96(0.08)	1.4(0.1)	1.75(0.08)	1.5(0.1)	1.9(0.1)

both the doubly and the singly charged species, are qualitatively similar to that of the corresponding homodimers. The symmetry of the mixed dimer is naturally lower (C_2) than that of the pure dimers. Again, the Na−K distances in the dianion and the monoanion are both shorter than the distance in bare NaK (3.59 Å).[33]

The predicted VDEs and ADEs at the B3LYP/tzvp+ level (Table 4) for the dianions are quite low (about 0.5 eV for the ADE's and about 0.6−0.8 eV for the VDE's) compared to the measured values. This is consistent with the results for KSO_4^- at the B3LYP/tzvp+ level where the calculated value is 0.3 eV lower than the experimental ADE and VDE. Furthermore, we note that the VDE of $NaSO_4^-$ is too low by 0.17 eV at the B3LYP/tzvp+ level. We expect that the dianionic nature of the

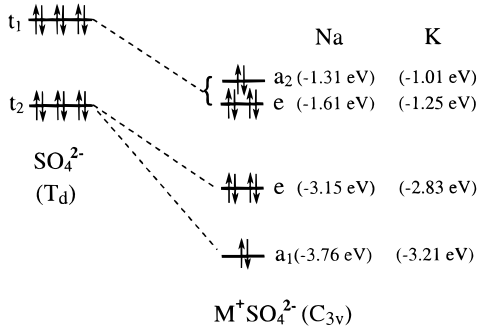

Figure 10. B3LYP/tzvp+ molecular orbitals and energies of $NaSO_4^-$ and KSO_4^- and their correlation to those of SO_4^{2-}.

dimers requires a more extensive theoretical treatment, such as a larger, more diffuse basis set and/or higher order correlation. The size of the dimers precluded single-point calculations at the CCSD(T)/6-311+G* level of theory, which would probably give a better agreement with the experimental values.

5. Interpretation of the Observed Photoelectron Features. The photoelectron spectral features represent transitions from the ground state of the anion (MSO_4^-) to states of the neutral (MSO_4) or from the ground state of the dianion $[(MSO_4)_2^{2-}]$ to those of the singly charged anion $[(MSO_4)_2^-]$. In the single-particle (Koopman's) approximation, the photoelectron features can be equated to removal of electrons from the occupied molecular orbitals (MOs) of the respective anions. Figure 10 shows the top few occupied MOs for the C_{3v} $NaSO_4^-$ and their orbital energies calculated at the B3LYP/tzvp+ level. The highest occupied MO (HOMO) of $NaSO_4^-$ is the a_2 orbital. The next orbital is the e orbital, which is only separated from the HOMO by 0.3 eV. The broad band at ~4 eV (X, Figure 1) in the $NaSO_4^-$ spectra should correspond to detachment from these two MOs. Therefore, the X band in Figure 1 in fact consists of two transitions, the major cause for its broad nature. The next occupied MO (HOMO-2) is also an e orbital and should correspond to the A band in Figure 1. The calculated energy differences between the top three occupied MOs are in excellent agreement with the experimental PES features.

Figure 10 also shows a correlation between the MOs of $NaSO_4^-$ and SO_4^{2-}. SO_4^{2-} exists in the condensed phase as an approximately tetrahedral unit.[7,8] SO_4^{2-} is unstable in the gas phase owing to the strong Coulomb repulsion between the excess charges.[9] The MSO_4^- complexes can be viewed as an SO_4^{2-} stabilized (and distorted) by an alkali metal cation through electrostatic interactions. The triply degenerate t_1 HOMO of SO_4^{2-} is split by the presence of the alkali metal in the ion pair in C_{3v} symmetry into the a_2 and e orbital in $NaSO_4^-$, corresponding to the X feature in Figure 1. Similarly, the triply degenerate t_2 orbital of SO_4^{2-} is split into an e and an a_1 orbital in $NaSO_4^-$. This e orbital becomes the HOMO-2 in $NaSO_4^-$, corresponding to the A feature in the PES spectra (Figure 1). The splitting of the t_2 MO of SO_4^{2-} is larger in $NaSO_4^-$, and the a_1 component is higher in binding energy (more stable) by 0.6 eV than the e component. The A feature in the PES spectra is narrower than the X feature, consistent with the fact that it consists of only one detachment channel. Detachment from the a_1 orbital in $NaSO_4^-$ will require a higher photon energy. These results show that the PES spectra of the ion pair reflect roughly the electronic energy levels of SO_4^{2-}.

The KSO_4^- PES is nearly identical to that of $NaSO_4^-$ except that its binding energies were lower by ~0.2 eV. This lowering of the binding energy in the KSO_4^- ion pair is due to the larger size of the K^+ ion, reducing the Coulomb attraction between

K^+ and SO_4^{2-}, as can be seen from the optimized structure of KSO_4^- (Figure 6). As expected, the calculated MO energy levels of KSO_4^- are similar to those of $NaSO_4^{2-}$ with smaller splittings (Figure 10). It is useful to note that the difference in Koopmann's theorem ionization energies for $NaSO_4^-$ and KSO_4^- is 0.3 eV, consistent with the experimental observation.

The PES spectra of the dimers showed identical features as the spectra of the monomers, suggesting that the dimers have similar energy levels as the monomers. The lowering of the binding energies in the dimers is due to the extra Coulomb repulsion between the two negative charges.

The observation of the dimer dianions was quite unexpected. Previously, Scheller et al. predicted theoretically that multiply charged anions of alkali metal fluoride salt bridge clusters would be stable in the gas phase.[34] As seen in Figures 1−3, the abundance of the dianions is quite low compared to the singly charged ion pairs. The structures of these dimer dianions are true salt bridge complexes. It is interesting to speculate on the existence of such salt bridge complexes in the solution phase under certain conditions, e.g., in concentrated solutions or in certain solvents.

V. Conclusion

We report the first gas-phase study of alkali metal sulfate ion pairs, $M^+(SO_4^{2-})$ (M = Na and K), and their dimer dianions. We produced these species in the gas phase using an electrospray technique and measured their photoelectron spectra, which provide direct information about their electron binding energies and electronic structure. We also carried out DFT and ab initio calculations on these novel gas-phase species to obtained further geometric and electronic structure data. The calculated electron binding energies for the MSO_4^- ion pairs are in good agreement with the experimental values. The MSO_4^- species have a C_{3v} ground state with a C_{2v} isomer higher in energy. The predicted geometries of the dimers can be viewed as two alkali metal cations bridging two SO_4^{2-} groups and thus can be truly called salt bridge complexes. The electronic features of the ion-pair complexes are all very similar and correlate well with the MO energy levels of "free" SO_4^{2-}. Thus, the complexes can be considered as a somewhat distorted "free" SO_4^{2-} interacting electrostatically with the alkali metal cations, as found in bulk sulfate solids. The electron binding energies of the dimer dianions are lower than the corresponding monomers owing to the Coulomb repulsion between the excess charges in the dianion cases. The repulsive Coulomb barrier against electron detachment, which exists in any multiply charged anions, was also observed in the dianions.

Acknowledgment. This work was supported by The U.S. Department of Energy, Office of Basic Energy Sciences, Chemical Science Division. Acknowledgment is also made to the Donors of The Petroleum Research Fund, administered by the American Chemical Society, for partial support of this research. Computer resources were provided by the Scientific Computing Staff, Office of Energy Research, at the National Energy Research Supercomputer Center (NERSC), Livermore, California. This research was performed at the W. R. Wiley Environmental Molecular Sciences Laboratory, a national scientific user facility sponsored by DOE's Office of Biological and Environmental Research and located at Pacific Northwest National Laboratory, which is operated for DOE by Battelle. L.S.W. is an Alfred P. Sloan Foundation Research Fellow.

References and Notes

(1) Hayon, E.; McGarvey, J. J. *J. Phys. Chem*. **1967**, *71*, 1472. Barrett, J.; Fox, M. F.; Mansell, A. L. *J. Phys. Chem*. **1965**, *69*, 2996. Halmann, M.; Platzner, I *J. Phys. Chem*. **1966**, *70*, 580.

(2) Hester, R. E.; Krishnan, K. *J. Chem. Phys*. **1968**, *49*, 4356. Walrafen, G. E. *J. Chem. Phys*. **1963**, *39*, 1479.

(3) Larson, A. C. *Acta Crystallogr*. **1965**, *18*, 717.

(4) Wu, G. J.; Frech, R. *J. Chem. Phys*. **1977**, *66*, 1352. Alvares, S.; Tabacik, V.; Cazabo, J. *J. Mol. Struct*. **1984**, *106*, 293.

(5) Zarzycki, J. *Discuss. Faraday Soc*. **1961**, *32*, 38.

(6) Iwadate, Y.; Mochinaga, J.; Kawamura, K. *J. Phys. Chem*. **1981**, *85*, 3708.

(7) Bishop, D. M.; Randic, M.; Morton, J. R. *J. Chem. Phys*. **1966**, *45*, 1880.

(8) Bishop, D. M. *Theor. Chim. Acta* **1967**, *8*, 285.

(9) Boldyrev, A. I.; Simons, J. *J. Phys. Chem*. **1994**, *98*, 2298. Stefanovich, E. V.; Boldyrev, A. I.; Truong, T. N.; Simons, J. *J. Phys. Chem. B* **1998**, *102*, 4205. Cannon, W. R.; Pettitt, B. M.; McCammon, J. A. *J. Phys. Chem*. **1994**, *98*, 6225.

(10) Blades, A. T.; Kebarle, P. *J. Am. Chem. Soc*. **1994**, *116*, 10761.

(11) Fleissner, G.; Hallbrucker, A.; Mayer, E. *J. Phys. Chem. B* **1998**, *102*, 6239 and references therein.

(12) Perutz, M. F. *Science* **1978**, *201*, 1187.

(13) Farnham, W. B.; Smart, B. E.; Middleton, W. J.; Calabrese, J. C.; Dixon, D. A. *J. Am. Chem. Soc*. **1985**, *107*, 4565.

(14) Dixon, D. A.; Farnham, W. B.; Heilemann, W.; Mews, R.; Noltemeyer, M. *Heteroatom* **1993**, *4*, 287.

(15) For a review see the following. Irish, D. E.; Brooker, M. H. In *Advances in Infrared and Raman Spectroscopy*; Clark, R. J. H., Hester, R. E., Eds.; Heyden: London, 1976; Vol. 2, Chapter 6.

(16) Walrafen, G. E. *J. Chem. Phys*. **1965**, *43*, 479.

(17) Ivanov, S. I.; Lupinetti, S. V.; Miller, S. M.; Anderson, O. P.; Solnstev, K. A.; Strauss, S. H. *Inorg. Chem*. **1995**, *34*, 6419. Van Seggen, D. M.; Hurlburt, P. K.; Anderson, O. P.; Strauss, S. H. *Inorg. Chem*. **1995**, *34*, 3453.

(18) Rudnyi, E. B.; Sidorov, L. N.; Vovk, O. M. *High Temp. USSR* **1985**, *23*, 238. Rudnyi, E. B.; Vovk, O. M; Kaibicheva, E. A.; Sidorov, L. N. *J. Chem. Thermodyn*. **1989**, *21*, 247.

(19) Wang, X. B.; Ding, C. F.; Wang, L. S. *Phys. Rev. Lett*. **1998**, *81*, 3351.

(20) Wang, L. S.; Ding, C. F.; Wang, X. B.; Nicholas, J. B. *Phys. Rev. Lett*. **1998**, *81*, 2667.

(21) Ding, C. F.; Wang, X. B.; Wang, L. S. *J. Phys. Chem. A* **1998**, *102*, 8633.

(22) Ding, C. F.; Wang, X. B.; Wang, L. S. *J. Chem. Phys*. **1999**, *110*, 3635.

(23) Wang, L. S.; Ding, C. F.; Wang, X. B.; Barlow, S. E. *Rev. Sci. Instrum*. **1999**, *70*, 1957.

(24) Hotop, H.; Lineberger, W. C. *J. Phys. Chem. Ref. Data* **1985**, *14*, 731.

(25) Becke, A. D. *J. Chem. Phys*. **1993**, *98*, 5648.

(26) The triple-ζ basis set is incorporated in DGauss and follows the polarized double-ζ basis set form given in the following. Godbout, N.; Salahub, D. R.; Andzelm, J.; Wimmer, E. *Can. J. Chem*. **1992**, *70*, 560.

(27) DGauss is available from Oxford Molecular, Beaverton, OR as part of the UniChem suite of programs.

(28) Hay, P. J.; Wadt, W. R. *J. Chem. Phys*. **1985**, *82*, 299.

(29) Glendening, E. D.; Feller, D.; Thompson, M. A. *J. Am. Chem. Soc*. **1994**, *116*, 10657.

(30) Mulliken, R. S. *J. Chem. Phys*. **1955**, *23*, 1833.

(31) Frisch, M. J.; Trucks, G. W.; Schlegal, H. B.; Gill, P. M. W.; Johnson, B. G.; Robb, M. A.; Cheeseman, J. R.; Keith, T.; Petersson, G. A.; Montgomery, J. A.; Raghavachari, K.; Al-Laham, M. A.; Zakrzewski, V. G.; Ortiz, J. V.; Foresman, J. B.; Cioslowski, J.; Stefanov, B. B.; Nanayakkara, A.; Challacombe, M.; Peng, C. Y.; Ayala, P. Y.; Chen, W.; Wong, M. W.; Andres, J. L.; Replogle, E. S.; Gomperts, R.; Martin, R. L.; Fox, D. J.; Binkley, J. S.; Defrees, D. J.; Baker, J.; Stewart, J. P.; Head-Gordon, M.; Gonzalez, C.; Pople, J. A. *Gaussian 94*, revision B.2; Gaussian, Inc.: Pittsburgh, PA, 1995.

(32) Wang, X. B.; Ding, C. F.; Wang, L. S. *Chem. Phys. Lett.*, submitted.

(33) Huber, K. P.; Herzberg, G. *Molecular Spectra and Molecular Structure: Constants of Diatomic Molecules*; Van Nostrand Reinhold Co. Inc.: New York, 1979.

(34) Scheller, M. K.; Compton, R. N.; Cerderbaum, L. S. *Science* **1995**, *270*, 1160.